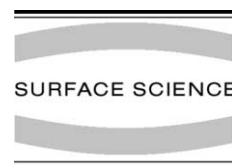




ELSEVIER

Surface Science 512 (2002) 269–280



www.elsevier.com/locate/susc

# Single domain Ca-induced reconstruction on vicinal Si(1 1 1)

D.Y. Petrovykh<sup>a,\*</sup>, K.N. Altmann<sup>a</sup>, J.-L. Lin<sup>a</sup>, F.J. Himpsel<sup>a,\*</sup>, F.M. Leibsle<sup>b</sup>

<sup>a</sup> Department of Physics, University of Wisconsin—Madison, 1150 University Avenue, Madison, WI 53706, USA

<sup>b</sup> Department of Physics, University of Missouri at Kansas City, 5110 Rockhill Road, Kansas City, MO 64110, USA

Received 9 November 2001; accepted for publication 1 April 2002

## Abstract

High-quality vicinal Si(1 1 1) surfaces are used as templates to create single domains of the Si(1 1 1) $\times$ 1-Ca reconstruction which exhibit atomic chains parallel to Si steps. Scanning tunneling microscope images support the formation of honeycomb chains of Si atoms, rather than zigzag chains proposed in earlier models. Angle-resolved photoemission is used to map out the dispersion of valence band states parallel and perpendicular to the chains. A gap of  $\approx$ 0.9 eV is found below the Fermi level with both in-plane and out-of-plane polarization of the synchrotron light. The observed semiconducting behavior suggests that the honeycomb chain channel model proposed for the alkali-induced  $3 \times 1$  reconstruction be modified for divalent alkaline earths, e.g. a  $3 \times 2$  structure with  $1/6$  monolayer coverage. © 2002 Elsevier Science B.V. All rights reserved.

**Keywords:** Synchrotron radiation photoelectron spectroscopy; Scanning tunneling microscopy; Surface electronic phenomena (work function, surface potential, surface states, etc.); Surface relaxation and reconstruction; Silicon; Alkaline earth metals; Vicinal single crystal surfaces

## 1. Introduction

Atomic scale objects are perhaps the most intriguing systems in nanotechnology. While building devices by manipulating individual atoms is still largely limited to fascinating one-of-a-kind experiments, there are structures with dimensions as small as a few atoms that can be created over

macroscopic areas by self-assembly. Among these are atomic chains which provide experimental approximations to truly one-dimensional (1D) systems [1].

Adsorbate-induced chain structures are often observed on surfaces. In particular, semiconductor substrates and metal adsorbates can be combined into systems with tailored electronic properties, including potential 1D metals [1]. There are two important advantages of semiconductor substrates: broken bonds, that often naturally rearrange into long-range anisotropic reconstructions, and band gaps, that reduce overlap between the bulk electronic structure and surface states close to the Fermi level.

An example examined in this paper is the Ca-induced  $3 \times 1$  reconstruction on Si(1 1 1) surface

\* Corresponding authors. Address: Naval Research Laboratory, Code 6177, Washington DC 20375-5342, USA. Tel.: +1-202-404-3381 (D.Y. Petrovykh)/+1-608-263-5590 (F.J. Himpsel); fax: +1-202-767-3321 (D.Y. Petrovykh)/+1-608-265-2334 (F.J. Himpsel).

E-mail addresses: dmitri@stm2.nrl.navy.mil (D.Y. Petrovykh), fhimpsel@facstaff.wisc.edu (F.J. Himpsel).

<sup>1</sup> Present address: Department of Physics, University of Maryland, College Park, MD 20742, USA.

(Si(1 1 1) $3 \times 1$ -Ca or Ca- $3 \times 1$  for brevity). It is very similar to Si(1 1 1) $3 \times 1$  reconstructions induced primarily by alkali metals (AM) [2] and alkaline-earth (AE) metals [3,4]. Note that, as discussed in Section 6, the structure may in fact be a  $3 \times 2$  rather than  $3 \times 1$  reconstruction. To avoid unnecessary confusion with the existing literature, we will refer to the structure as Ca- $3 \times 1$  in this paper and relegate the discussion of the true periodicity to Section 6. An electron count based on the structural models for the  $3 \times 1$  unit cell suggests a possibility that Ca- $3 \times 1$  is a metallic quasi-1D system. The Si atoms supply an odd number of electrons: three in models with four Si atoms per unit cell in a chain structure [5,6], five in models with five Si atoms in a honeycomb chain structure [6]. Each AM atom then donates an additional electron making for an even total electron count and thus an insulating system (in agreement with photoemission measurements [5,6]). Assuming a similar structure, the addition of an extra electron per unit cell by the divalent Ca would produce a half-filled metallic state.

In the next section the preparation of the single-domain Si(1 1 1) $3 \times 1$ -Ca samples is discussed in detail. Our vicinal Si(1 1 1) substrates were prepared to have arrays of steps with very few kinks thus ensuring the formation of  $3 \times 1$  domains along the step direction. This surface preparation has been characterized by scanning tunneling microscopy (STM), low energy electron diffraction (LEED) and photoemission (PES). Section 3 discusses the appearance of individual  $3 \times 1$  rows in the high-resolution STM images. Observations are consistent with a honeycomb chain of Si atoms, as suggested by recent models [6], whereas a perhaps more intuitive zigzag chain of atoms model [5] is ruled out. The Ca coverage in the Ca- $3 \times 1$  reconstruction is discussed in Section 4. In Section 5 the angle-resolved photoemission (ARPES) data obtained using synchrotron radiation with both in-plane and out-of-plane polarization is presented and compared to other published results [3,7,8]. No metallic state is observed, so the simple generalization of the AM- $3 \times 1$  structure apparently fails and we consider possible modifications suggested by our data as well as by recent results from other groups. These

considerations, together with our conclusions, are presented in Section 6.

## 2. Single-domain Si(1 1 1) $3 \times 1$ -Ca preparation

Typically, metal-induced  $3 \times 1$  reconstructions on Si(1 1 1) surfaces are obtained by direct deposition of the respective metals. Ca deposition, however, produces several reconstructions [7,8], so even with good control of the coverage and temperature windows, a pure  $3 \times 1$  phase is not guaranteed [8]. The method that we choose to prepare our surfaces is to anneal Si(1 1 1) surfaces with sub-monolayer coverages of CaF<sub>2</sub>. This results in conversion to Ca- $3 \times 1$  [3], which is the favored structure above 700 °C [8] and is thus formed exclusively. Areas of clean Si on the surface can affect the PES data, in particular the intensity close to the Fermi level. CaF<sub>2</sub>-to-Ca- $3 \times 1$  conversion makes it easier to ensure the saturation coverage for the  $3 \times 1$  structure, because any small excess of CaF<sub>2</sub> can be removed using the procedure described later in this section.

Si(1 1 1) samples with a 1.1° miscut towards the ( $\bar{1}\bar{1}2$ ) azimuth were used as substrates. A special preparation procedure described in detail elsewhere [9] produced high quality stepped surfaces with single-domains of the Si(1 1 1) $7 \times 7$  reconstruction over at least  $\approx 1 \mu\text{m}^2$  areas. CaF<sub>2</sub> was deposited from a BN crucible evaporator onto substrates held typically at  $\approx 700$ – $730$  °C. Sample temperatures were determined using a Minolta–Land Cyclops 52 optical pyrometer (0.4 emissivity setting). We used the atomic density of the bulk-terminated Si(1 1 1) surface ( $7.8 \times 10^{14}$  atoms/cm<sup>2</sup>) to define 1 monolayer (ML). CaF<sub>2</sub> deposition rate was between 2 and 3 ML/min, within the range investigated in our previous study of CaF<sub>2</sub> growth modes on vicinal Si(1 1 1) [10]. Measurements of the CaF<sub>2</sub> and Ca coverages are discussed in detail in Section 4.

For CaF<sub>2</sub> coverages between 0.1 and 0.3 ML, the conversion to Ca- $3 \times 1$  above 700 °C is well documented [3,11,12]. Our STM and LEED observations show that, for CaF<sub>2</sub> coverages as high as 0.5–0.7 ML, the Ca- $3 \times 1$  layer is formed with

any excess  $\text{CaF}_2$  remaining as  $\text{CaF}_2$  islands attached to the top edges of steps. In annealing studies, the  $\text{CaF}_2$  islands are observed at lower and upper step edges before and after the  $\text{Ca-}3 \times 1$  conversion respectively, so in the latter case they are most likely positioned on top of the  $\text{Ca-}3 \times 1$  interface layer. These  $\text{CaF}_2$  islands can be removed by annealing the surface to 800–850 °C. Monitoring the single-domain  $3 \times 1$  LEED pattern throughout several series of high-temperature anneals suggests that the  $3 \times 1$  structure is stable up to  $\approx 925$  °C and is completely removed only above  $\approx 975$  °C which implies stability comparable to the  $\text{Si}(111)7 \times 7$  structure.

The above preparation produces a pure single-domain  $\text{Ca-}3 \times 1$  structure oriented parallel to steps ( $\bar{1}10$  direction). LEED and STM observations do not show any evidence of other rotationally-equivalent domains. The stepped Si substrates ensure the single-domain growth of  $\text{Ca-}3 \times 1$  in two ways. First, the steps break the three-fold surface symmetry (the few kinks that are present do not offer sufficient nucleation sites for alternative orientations). Second, the typical domain size is conserved during the  $\text{Si-}7 \times 7$  to  $\text{Ca-}3 \times 1$  conversion [11,12], so single-domain  $7 \times 7$

surfaces are converted into single-domain  $3 \times 1$  surfaces.

Fig. 1 illustrates the effects of this preparation procedure: shown on the left are images from clean single-domain  $\text{Si}(111)7 \times 7$  stepped surfaces, shown on the right are corresponding images from single-domain  $\text{Ca-}3 \times 1$  formed on these surfaces. Derivative views of the STM images are used to emphasize the steps (dark lines) and the periodicities of the reconstructions. The  $\text{Ca-}3 \times 1$  reconstruction appears in Fig. 1(b) and (d) as row-like structures parallel to the steps ( $3a$  spacing is resolved,  $a = 0.38$  nm). Compared to a well-defined array of straight single steps shown in Fig. 1(a), meandering step edges and corresponding increased variation of terrace widths in Fig. 1(b) indicate significant motion of Si steps caused by the formation of  $\text{Ca-}3 \times 1$  domains. In larger area images a number of wandering steps are also present (not shown). This step motion is an adsorbate-induced effect, which has been previously observed in reflection electron microscopy studies [11]. The single-domain  $\text{Ca-}3 \times 1$  structure however is established by the initial nucleation at straight steps, so it is preserved when steps are pushed by growing  $\text{Ca-}3 \times 1$  domains [11].

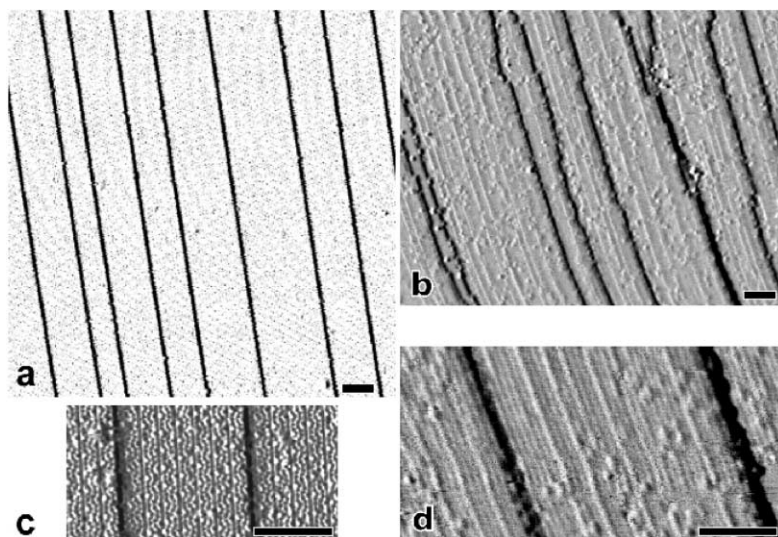


Fig. 1. Stepped  $\text{Si}(111)7 \times 7$  surfaces (a,c) serve as templates for forming a single-domain  $\text{Si}(111)3 \times 1$ -Ca reconstruction oriented parallel to steps (b,d). The  $x$ -derivative of the topography is shown to emphasize the  $7 \times 7$  and  $3 \times 1$  reconstructions, and the substrate steps (dark lines). Scale bars are 10 nm.

In addition to LEED and STM, we have also characterized the  $\text{Ca-3} \times 1$  preparation sequence by following the surface composition signatures in the core-level and valence-band angle-integrated photoemission spectra (Fig. 2). The top spectrum in Fig. 2 corresponds to a  $\text{CaF}_2$  submonolayer (compare Fig. 4 in Ref. [13]). It shows a single F 2p peak, Ca 3p peak with nearly stoichiometric Ca/F ratio, and discernible Si valence band features. After the conversion to the  $\text{Ca-3} \times 1$  interface at  $\approx 730^\circ\text{C}$ , the Ca/F peak ratio increased (i.e. less F was present) and the relative intensity of the Si valence band peaks increased (i.e. total  $\text{CaF}_2$  coverage was reduced). From our STM study, we knew that this stage corresponded to  $\text{Ca-3} \times 1$  surfaces with a small number of  $\text{CaF}_2$  islands. A shift of the F 2p peak to higher binding energy supports this interpretation, since the higher F 2p binding energy is likely due to reduced screening in bulk-like  $\text{CaF}_2$  islands compared to the  $\text{CaF}_2$ -Si(111) interface [13]. An additional 20 s anneal

between 800 and 850  $^\circ\text{C}$  removed the remaining  $\text{CaF}_2$  islands, resulting in a clean  $\text{Ca-3} \times 1$  surface with the Ca 3p peak still present but no F peak left. The high cross-section for the F 2p peak makes this method very sensitive to F [3]. We note that the valence-band structure for  $\text{Ca-3} \times 1$  surfaces is significantly altered from that for clean Si(111) $7 \times 7$  surfaces (bottom spectrum in Fig. 2). The clearly visible surface states in the clean Si(111) $7 \times 7$  spectrum (shaded) indicate the high quality of the original substrate. ARPES results for valence-band and surface states are presented in Section 5.

### 3. Si(111) $3 \times 1$ -Ca structure

There is a whole class of Si(111) $3 \times 1$ -M reconstructions that are primarily induced by alkali [2] and AE [3,4] metals but also have been observed for Ag [14,15], Yb [16,17] and Sm [17,18]. Essentially the same reordering of the Si substrate in the Si(111) $3 \times 1$ -M systems is suggested by results from a variety of techniques: STM comparison studies [14,19], transmission diffraction [20], surface X-ray diffraction [21], LEED [4,22], and core-level spectroscopy [6,23].

In agreement with other STM studies, we find that the filled state images with atomic resolution show zigzag chains (Fig. 3 bottom). The intuitive idea is that the bright protrusions correspond to orbitals of a chain of Si atoms (or perhaps other atoms attached to a Si chain). The generalized schematic of such a model is shown in Fig. 3 (top left) together with an overlay on a filled state STM image (bottom left). A good example from this class is the Seiwatz model that has been examined by both experiments and theory [5,6,24].

Images of a sample with co-existing  $3 \times 1$  and  $7 \times 7$  regions (Fig. 4) suggest however that the structure is actually more complicated. This sample was prepared by  $\text{CaF}_2$  deposition at  $\approx 550^\circ\text{C}$  on a surface with wide terraces, followed by annealing to achieve the  $\text{CaF}_2$  to  $\text{Ca-3} \times 1$  conversion. The  $\text{CaF}_2$  coverage was less than that required for the full  $\text{Ca-3} \times 1$  layer.

The images in Fig. 4 show a boundary between  $7 \times 7$  and  $3 \times 1$  regions (Fig. 4 left) and an internal

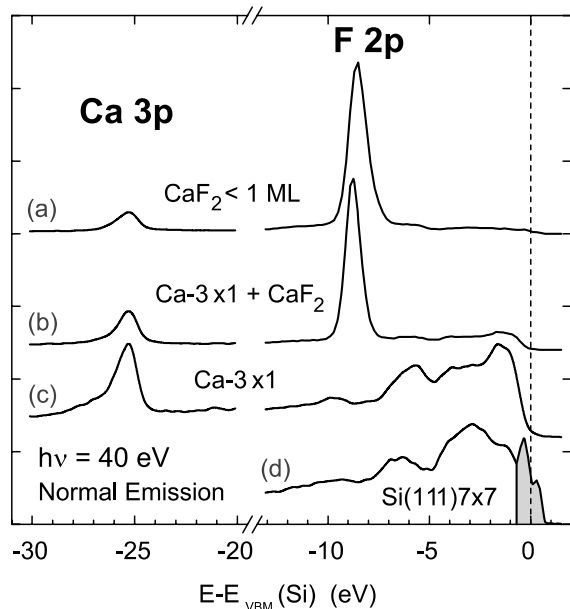


Fig. 2. Photoemission signatures of the  $\text{CaF}_2$  to  $\text{Ca-3} \times 1$  conversion, from top to bottom: (a) a submonolayer of  $\text{CaF}_2$  on Si(111), (b) Si(111) $3 \times 1$ -Ca with  $\text{CaF}_2$  islands after conversion at  $\approx 730^\circ\text{C}$  (higher Ca/F and Si/F peak ratios), (c) Si(111) $3 \times 1$ -Ca after the  $\text{CaF}_2$  islands have been removed by an anneal at 800–850  $^\circ\text{C}$  and (d) the clean Si(111) $7 \times 7$  surface for comparison (surface states shaded).

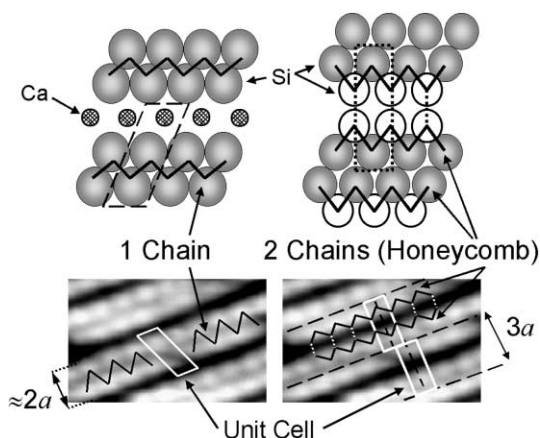


Fig. 3. Two types of structural models proposed for metal-induced Si(111) $3 \times 1$  structures, one containing a single zigzag chain, the other containing a pair of opposing zigzag chains with extra Si atoms (o) arranged as a honeycomb chain. Both types of chains are composed of Si atoms. The STM data in Fig. 4 favor models with two chains.

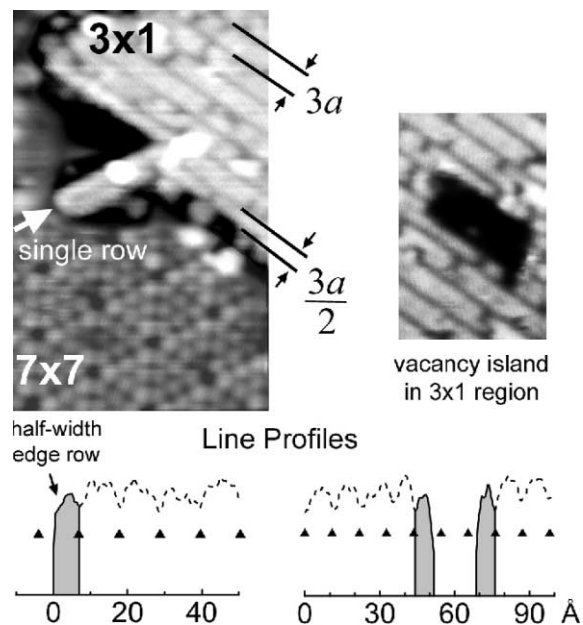


Fig. 4. Decomposition of the  $3 \times 1$  unit cell into two chains. Stripes at the boundaries of the bright  $3 \times 1$  regions are only half as wide as the  $3 \times 1$  unit cell. The reduced width of these edge rows is confirmed by line profiles (bottom). An isolated row is marked on the top left. These observations favor models with two chains per unit cell (see Fig. 3). The sample bias is  $-2.75$  V.

boundary around a vacancy island in the middle of a  $3 \times 1$  region (Fig. 4 right). By simple visual inspection and by looking at the corresponding line profiles, it is clear that this “edge row” (shaded in line profiles) has a width of only about half of the  $3a$  periodicity measured from the adjacent rows (triangular markers).

The rest of the  $3 \times 1$  structure appears as bright  $\approx 7$  Å wide stripes separated by narrow dark gaps. The most natural way to reconcile the observation of the regular width rows in the middle of the  $3 \times 1$  region and the half-width “edge rows” was suggested in studies of AM- $3 \times 1$  [25,26]. The idea is that a single row of the  $3 \times 1$  reconstruction consists of *two* chains (Fig. 3 right), which appear as *two* bright lines. In fact, there is one feature with that appearance marked in the middle of the left image in Fig. 4 and it indeed looks like a split-off individual row. In the middle of the  $3 \times 1$  regions, gaps between rows are not resolved and pairs of chains from *adjacent* rows appear as wide bright stripes. On the boundaries, respectively one of the two chains in a  $3 \times 1$  row is resolved and appears as an “edge row” feature described above. Position of Ca atoms (e.g. between vs. on top of chains) cannot be determined from the filled state STM images, so they are not included in the schematic in Fig. 3 (right).

Two opposing zigzag chains of Si atoms arranged as a honeycomb chain are proposed in the “honeycomb chain-channel” (HCC) model [20,21,27], which in fact predicts for Li- $3 \times 1$  that individual rows appear as two bright lines [27]. Very similar result for the empty state images has been recently calculated in Ref. [28] for the Ba-induced structure based on the HCC model. The peculiar appearance of the stand alone and edge rows shown in Fig. 4 is thus clearly consistent with the HCC predictions. The apparent similarity between the results for AM and divalent Ba and Ca does not extend however to the electronic structure, which we discuss in Section 5.

#### 4. CaF<sub>2</sub> and Ca coverage measurements

STM images provided the most accurate way to measure CaF<sub>2</sub> coverages in this study. On vicinal

surfaces deposition at 600–650 °C produces CaF<sub>2</sub> islands [10] in contrast to growth on flat Si(1 1 1) where a Si–Ca–F interface is formed at these temperatures. The two types of interface can be easily distinguished in STM images because CaF<sub>2</sub> and Si–Ca–F structures preferentially attach to lower and upper step edges respectively [10]. The height of CaF<sub>2</sub> islands in STM images is affected by electronic structure effects [10], e.g. at +4 V sample bias, required for stable imaging, they appear higher than single Si steps. Characteristic appearance of CaF<sub>2</sub> islands allows accurate measurement (typically <10% variation between images) of their total area, which for submonolayer depositions is proportional to deposition time and is consistent with actual island height of 1 CaF<sub>2</sub> layer. These data were used to calibrate the deposition rate for stoichiometric CaF<sub>2</sub>, and to calculate the CaF<sub>2</sub> flux and effective coverages for depositions at higher substrate temperature where direct STM measurements could not be done.

To determine the CaF<sub>2</sub> coverage required for a saturated Ca-3 × 1 layer formation, CaF<sub>2</sub> was deposited at 600–650 °C as described above. Such samples were then annealed at about 750 °C and showed a 3 × 1 LEED pattern and a 3 × 1 reconstruction in STM images (e.g. see Fig. 1). Samples with initial coverage below 1/3 ML of CaF<sub>2</sub> contained areas of Ca-3 × 1 and clean Si after the conversion. Coverage above 1/3 ML produced Ca-3 × 1 surfaces with excess CaF<sub>2</sub> in islands on upper step edges. These observations indicate that one needs to start with 1/3 ML of CaF<sub>2</sub> in order to produce a saturated Ca-3 × 1 layer and that about 1/3 ML of CaF<sub>2</sub> is consumed during the conversion in this preparation sequence (consistent with the previous reports for this method [3]). PES spectra corresponding to a similar sequence were discussed in Section 2 (Fig. 2).

CaF<sub>2</sub> deposition followed by post-annealing is not always reliable in producing pure single-domain 3 × 1 reconstruction, because the domain structure depends on the morphology of the initial CaF<sub>2</sub> incomplete monolayer. In contrast, deposition at higher temperature (700–730 °C), where CaF<sub>2</sub> to Ca-3 × 1 conversion occurs directly, produces a pure single-domain 3 × 1 reconstruction on vicinal surfaces desirable for ARPES

experiments. In the high-temperature approach however, we could not measure the CaF<sub>2</sub> coverage directly. Using identical evaporator parameters, we obtained results consistent with those from lower-temperature deposition method, i.e. 1/3 ML of CaF<sub>2</sub> required for saturation Ca-3 × 1 coverage.

The bonding at the CaF<sub>2</sub>–Si(1 1 1) interface [3,13] translates 1/3 ML of CaF<sub>2</sub> into 1/3 ML of Ca coverage. The main caveat of these STM measurements is that they give no information about the Ca coverage in the Ca-3 × 1 structure, which may change from the initial CaF<sub>2</sub> coverage during the conversion and post-annealing. Ca atoms are not observed directly in filled state STM images, so we do not have direct means to estimate the final Ca coverage from the STM data.

The second method for measuring the Ca and CaF<sub>2</sub> coverage is from Ca 3p and F 2p core-level peak intensities in the PES data (Fig. 2). We used Si valence band features for normalizing the spectra, because the Si 2p core-level peak, typically used for such normalization [13], was outside of the energy range of our PES experiments.

As described in Section 2, the annealing sequence shown in Fig. 2 corresponds to a conversion of a CaF<sub>2</sub> submonolayer to a Ca-3 × 1 layer with CaF<sub>2</sub> islands during the first step (spectra (a) and (b) respectively) and complete desorption of the remaining CaF<sub>2</sub> in the second step (between spectra (b) and (c)). The two annealing steps produced a decrease by a factor of 2.5 and complete elimination of the F 2p peak respectively, corresponding Ca 3p peak reduction was 10–15% and 50%. We also note that the Si valence band region does not change dramatically during the second annealing step, so it does not substantially change the Ca-3 × 1 structure, but at the same time observed reduction in Ca amount is rather reliable even with the imperfect normalization.

The actual value of the final Ca coverage for the Ca-3 × 1 structure depends on the initial amount of CaF<sub>2</sub>. From evaporator calibration, we estimate that the initial amount was ≈0.4 ML of CaF<sub>2</sub>, giving the final Ca coverage close to 1/6 ML. The most conservative uncertainty estimate however puts the upper limit of the final Ca coverage at 1/3 ML, based on comparison to a sample with the highest amount of CaF<sub>2</sub> still consistent with less

than 1 ML of  $\text{CaF}_2$ . Our evaporator was calibrated to ensure sufficient initial  $\text{CaF}_2$  coverage, therefore any discrepancy is likely to be towards higher values.

The Ca coverage of 1/6 ML for the saturated  $\text{Ca-3} \times 1$ , favored by our PES data, is in agreement with a value of  $\approx 0.1$  ML of Ca, obtained by Olmstead et al. from core-level peak intensities for a 3 ML  $\text{CaF}_2$  film and the  $\text{Ca-3} \times 1$  surface [3]. It is important to note that a preparation procedure very similar to our sequence in Fig. 2 (i.e. annealing of a  $\text{CaF}_2$  submonolayer) was used to obtain the  $\text{Ca-3} \times 1$  in Ref. [3].

Comparison of the available data on the Ca and F coverage highlight the poor understanding of the complicated details of the  $\text{CaF}_2$  to  $\text{Ca-3} \times 1$  conversion process and corresponding intermediate  $\text{CaF}_x$ -Si interface structures at higher temperatures [29]. For example, in our experiment the Ca coverage dropped during the second annealing step, rather than during the  $\text{CaF}_2$  to  $\text{Ca-3} \times 1$  conversion, where it might be expected from naïve interpretation of the STM and LEED data. Also, observed evolution of the Ca and F amounts varies depending on initial  $\text{CaF}_2$  film thickness and morphology and details of annealing procedures, e.g. our results in Fig. 2 differ from those obtained in Refs. [3] and [29] in a similar procedure starting from a 3 ML  $\text{CaF}_2$  film.

The major implication of the Ca coverage in the  $\text{Ca-3} \times 1$  reconstruction is, of course, for electronic structure. As discussed in the introduction and the following sections, 1/3 ML coverage should produce a metallic surface, whereas 1/6 ML would maintain the same electron count as the alkali-induced  $3 \times 1$  and thus be semiconducting.

## 5. Si(111) $3 \times 1$ -Ca surface states

We used synchrotron radiation ARPES to identify  $\text{Ca-3} \times 1$  surface states and analyze their dispersion. Our data were acquired with a hemispherical Scienta SES200 spectrometer equipped with angle and energy multidetection and coupled to a Normal Incidence Monochromator beamline at the SRC. The angle between the incoming photons and the axis of the electron

spectrometer was kept fixed at  $50^\circ$ . Spectra were acquired with 0.1 eV energy resolution and 15 and 20 eV photon energy to optimize the signal-to-noise for the states of interest. Angular resolution was  $0.3^\circ$  (within the  $12^\circ$  multidetection range of the Scienta analyzer). The multidetection in energy and take-off angle produces photoelectron intensity maps where band dispersion can be tracked qualitatively and quantitatively across a large range in  $k$ -space (within  $\approx 8$  eV below the  $E_F$  and up to  $60^\circ$  off-normal in this study).

The  $\text{Ca-3} \times 1$  samples were prepared using the procedure described in Section 2. The single-domain  $\text{Ca-3} \times 1$  structure is very beneficial for the ARPES experiments because measurements can be carried out parallel and perpendicular to the rows without potential scrambling of spectral features by contributions from the other two domain orientations present on flat surfaces. Other potential sources of PES signal in the valence band region (and in particular close to the Fermi level) are areas with different Ca-induced reconstructions (e.g.  $5 \times 1$  and  $2 \times 1$  [8]) and clean Si. Our preparation procedure however very reliably produces exclusively the  $3 \times 1$  reconstruction with saturation coverage, as discussed in Section 2, so the resulting samples are particularly well suited for ARPES experiments.

For the first series of spectra we have used 15 eV energy photons with in-plane light polarization, i.e. the electric field of the photons parallel to the emission plane. After comparing band dispersion maps along the steps (and  $3 \times 1$  chains) for Si- $7 \times 7$  and  $\text{Ca-3} \times 1$ , we find one strong band that only appears for the  $\text{Ca-3} \times 1$  surface (shaded peak in Fig. 5) and is located in a gap between Si states, so it can be identified as a  $\text{Ca-3} \times 1$  state. The dispersion of this state (CS1) parallel to  $3 \times 1$  chains is shown in Fig. 6 (thick line and large full circles). The band clearly disperses  $\approx 0.5$  eV downwards from the  $\Gamma$  point to  $\approx 0.6 \text{ \AA}^{-1}$  (between  $\Gamma$  and A). Further towards A and K points the band is flattening and closely following a state seen for clean Si- $7 \times 7$ , so its identity becomes more ambiguous.

It has been suggested [27] that some  $3 \times 1$  surface states can be suppressed in photoemission spectra because the  $3 \times 1$  structure has an

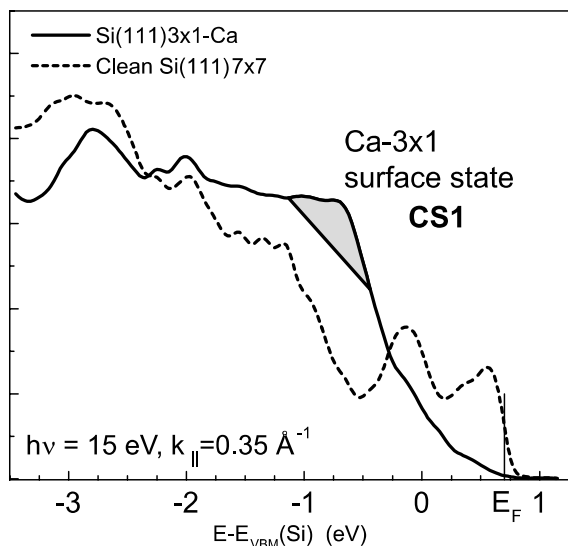


Fig. 5. ARPES of Si(111)3 × 1-Ca and Si(111)7 × 7 at  $k_{\parallel} = 0.35 \text{ \AA}^{-1}$  along the rows ( $\Gamma A$  in Figs. 6 and 7). A Ca-induced state (shaded) is observed in the gap between Si states. Photon energy  $h\nu = 15 \text{ eV}$ , in-plane polarization.

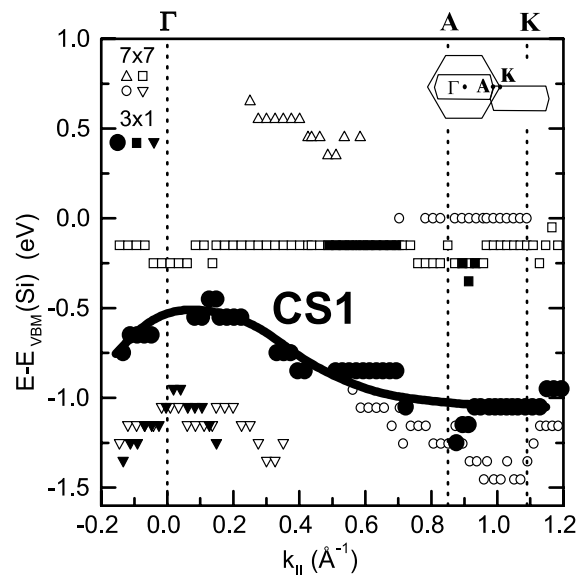


Fig. 6. Band dispersion parallel to rows for Si(111)3 × 1-Ca (full symbols) and Si(111)7 × 7 (open symbols). A Ca-induced state (CS1—full circles) disperses downward from  $-0.4 \text{ eV}$  at  $\Gamma$  to  $-1.05 \text{ eV}$  at A. The energy is referenced to the valence band maximum ( $E_{\text{VBM}}$ ) of Si. The Fermi level  $E_{\text{F}}$  is at  $0.65 \text{ eV}$  for Si(111)7 × 7 and at  $0.60 \text{ eV}$  for Si(111)3 × 1-Ca. Photon energy  $h\nu = 15 \text{ eV}$ , in-plane polarization.

approximate mirror symmetry plane, which in the in-plane polarization geometry (typical for synchrotron ARPES experiments) is parallel to the polarization of the incident light. To address this issue, we carried out an experiment in a modified geometry with analyzer (emission plane) rotated by  $90^\circ$ . We refer to this modified arrangement as out-of-plane polarization geometry, because the electric field of the photons is perpendicular to the emission plane in this configuration.

The change in polarization and photon energy ( $20 \text{ eV}$  for this series) allows us to clearly observe a Ca-3 × 1 band not identified in the above series. Fig. 7 shows the tentative outline of this surface band (CS2), with ARPES peak positions indicated by large full circles. Using the dispersion data from Figs. 6 and 7, weaker features (not shown) in the out-of-plane and in-plane polarization datasets can be identified with respectively CS1 and CS2. This allows us to check that the binding energies for CS1 and CS2 do not change with photon energy, thus confirming the surface character of both states.

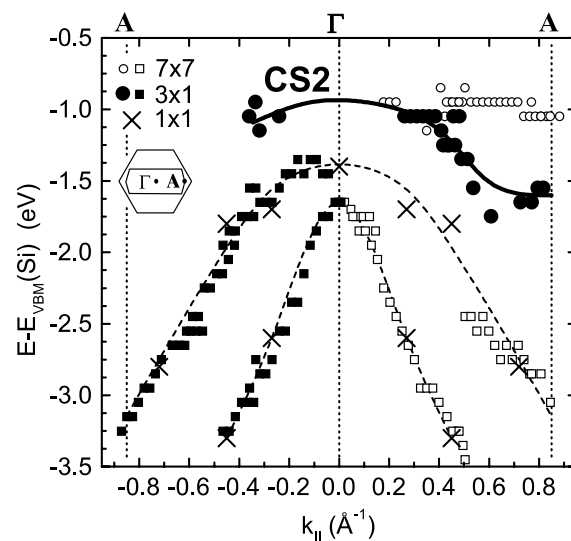


Fig. 7. Similar to Fig. 6, but with out-of-plane polarization and  $h\nu = 20 \text{ eV}$ . A second Ca-induced state is found (CS2—full circles) that disperses downward from  $-1.0 \text{ eV}$  at  $\Gamma$  to  $-1.55 \text{ eV}$  at A. Two bands at lower energy (dashed lines) point correspond to bulk Si states. Neither of the two Ca-induced states changes with photon energy (not shown), confirming their surface character.

The two strongly dispersing bands below  $-1.5$  eV in Fig. 7 (dashed lines, open (Si- $7 \times 7$ ) and full (Ca- $3 \times 1$ ) squares) are Si substrate bands previously reported in Ref. [30] for Si(1 1 1) $1 \times 1$ -As (several large X's in Fig. 7) and in our case observed with higher resolution in angle. Portions of the two bands for Ca- $3 \times 1$  (Si- $7 \times 7$ ) are shown in full (open) squares for negative (positive) values of  $k$  only, the counterparts symmetric around  $\Gamma$  are omitted for clarity. The higher binding energy band with steeper dispersion symmetric around  $\Gamma$  is used to align the band structure for Ca- $3 \times 1$  and clean Si in angle (i.e. find the true sample normal) and in energy (there is a small  $\approx 0.1$  eV Fermi level shift). Similarly, the datasets in Fig. 6 are aligned using the features at  $\approx -1$  eV near the  $\Gamma$  point and just below 0 eV between  $\Gamma$  and A.

To confirm the 1D character of the CS1 and CS2 surface states from Figs. 6 and 7, they should have very weak dispersion in the perpendicular direction. Unfortunately, we did not observe the counterparts for CS1 and CS2 along this direction using either of the above two light polarization and energy combinations. In fact, the valence bands observed for the Ca- $3 \times 1$  and the clean Si are remarkably similar (albeit peaks are often sharper for the Ca- $3 \times 1$ ). The only substantial difference between the two surfaces is in the region shown in Fig. 8. A band, that has a very shallow dispersion and is located in a gap between the Si states (open

and full squares), appears for the Ca- $3 \times 1$  between the C and M critical points of the  $3 \times 1$  Brillouin zone. Deep-lying bands with shallow dispersion perpendicular to the  $3 \times 1$  rows have been reported in a previous study of the Si(1 1 1) $3 \times 1$ -K [5], so it is likely that this band is associated with the  $3 \times 1$  reconstruction. Because of the broadening associated with the high binding energy however, the distinction between the surface and bulk character of this state becomes ambiguous.

In a recently published study of a three-domain Ca- $3 \times 1$  surface, two features were reported in the angle-integrated valence band spectrum (labeled D1 and D2 in Fig. 9 of Ref. [8]). The shape of that integrated spectrum generally agrees with our data, especially with that acquired using the in-plane light polarization where the features are more pronounced around the  $\Gamma$  point (Fig. 6). We also agree with the assignment of the lower peak to the Si substrate bonds (D2 at  $\approx 1.6$  eV below  $E_F$  in [8] and a band respectively at  $\approx 1$  eV below VBM near  $\Gamma$  in Fig. 6). The higher lying state, marked D1 in [8] and CS1 in Fig. 6, is according to our results Ca-induced, and thus is possibly due to Ca-Si bonds as suggested in Ref. [8].

In addition to the observation of the two Ca- $3 \times 1$  surface states CS1 and CS2 shown in Figs. 6 and 7, the most important observation from our spectra is that the Ca- $3 \times 1$  surface is a semiconductor, with a gap of about 0.9–1.0 eV below the Fermi level measured in all of the experimental configurations. Angle-integrated spectrum in Ref. [8] shows an apparent band gap slightly less than 1 eV below  $E_F$  (synchrotron  $h\nu = 55$  eV, sample  $T = -172$  °C), Ref. [3] also reports no metallic edge (He I lamp  $h\nu = 21.2$  eV). Given a multi-domain nature of the Ca- $3 \times 1$  surfaces in [3] and [8] as well as different photon energies and temperatures, together with our data we have definite evidence of the semiconducting nature of the Ca- $3 \times 1$  surface.

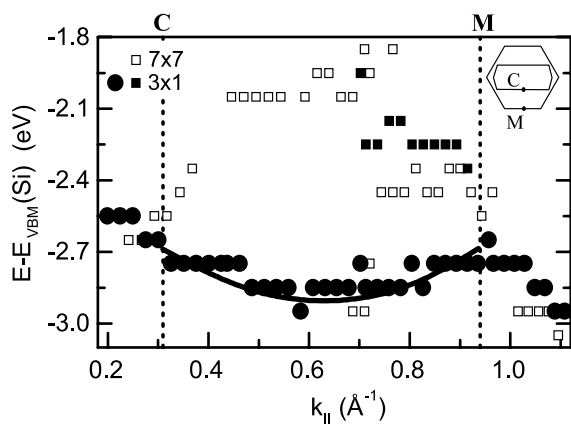


Fig. 8. A Ca-induced state with weak dispersion perpendicular to the  $3 \times 1$  rows ( $\bullet$ ) which indicates nearly one-dimensional character.  $h\nu = 15$  eV, in-plane polarization.

## 6. Discussion and conclusions

The HCC model has been remarkably successful in accounting for the experimental results obtained by a variety of techniques for alkali metal induced

$3 \times 1$  reconstructions. Given the similarities in LEED, STM and Si 2p core-level observations in studies of AE and alkali-induced  $3 \times 1$  structures, it is only reasonable to assume a similar structure.

First, let us consider the STM results. Our analysis, in particular the “edge row” observation (Section 3), is consistent with the HCC structure. The HCC structure is also favored by the density of the outermost Si atoms determined in Ref. [31] for several  $3 \times 1$  reconstructions, including the Mg- and Ca- $3 \times 1$ . STM images and core-level spectra for the Ca-induced reconstructions are explained in terms of the HCC and its appropriate combinations with other structures in Ref. [8]. STM images very similar to those for the Mg- and Ca- $3 \times 1$  have been recently reported for the Ba-induced structure [28].

In photoemission, the two bands that we observe for Ca- $3 \times 1$  (CS1 and CS2 in Figs. 6 and 7) have dispersions similar to two bands reported for Mg- $3 \times 1$  (labeled  $SS'_1$  and  $SS'_2$  in Fig. 3 of Ref. [32]) and bands observed for Ba- $3 \times 1$  [33]. Note that the dispersions observed for these bands for Ba-, Mg- and Ca- $3 \times 1$  are also comparable to the calculated dispersions of two bands in Li- $3 \times 1$  (labeled  $S_1^+$  and  $S_2^+$  in Fig. 2 of Ref. [27]). According to results of Ref. [27], these two states are related to the special features of the HCC model. Their observation for Ca- $3 \times 1$  and other alkaline earth-induced  $3 \times 1$  surfaces suggests that the basic HCC backbone is still present. Furthermore, these states determine the appearance of the STM images for filled states [27], and images are again similar for alkalis and alkaline earths [28,31–33].

While providing strong circumstantial evidence for the HCC reconstruction of the silicon substrate, the photoemission data also suggest a difference in the number of alkali and alkaline earth atoms incorporated into this backbone. The alkali metal induced  $3 \times 1$  is predicted to be a semiconducting surface and appears so in photoemission spectra [5,6]. Simple substitution of monovalent alkali atoms with divalent alkaline earth metal atoms would raise the electron count by one and produce a metallic surface in marked disagreement with the experimental evidence that the alkaline earth induced  $3 \times 1$  surfaces remain semiconducting (Section 5, [3,8,32,33]).

The most generic mechanism for destroying the metallic 1D states is doubling of the periodicity [1] by a Peierls-like distortion. One LEED study [7] reported half-order streaks indicative of a  $3 \times 2$  Ca-induced structure. Empty state STM images showing the  $3 \times 2$  periodicity have been reported for Ca [7,8,31], Mg [31,34] and Ba [28]. However, as explained above, the filled state STM images and PES data suggest that the Si lattice of the HCC structure is not significantly modified (especially given the major buckling that would be required to account for the observed  $\approx 1$  eV gap by Peierls distortion alone).

A very elegant explanation consistent with both of the above constraints has been recently suggested for the Ba-induced system [28]. The absolute Ba coverage measured by medium-energy ion scattering (MEIS) is 1/6, rather than 1/3 ML, i.e. one Ba atom per two unit cells of the HCC. The resulting structure is then  $3 \times 2$  and the properties of the Si lattice are similar to that of the alkali-induced  $3 \times 1$ , since the electron count is the same. The even electron count explains the semiconducting gap as well. The calculated band gap for the Ba- $3 \times 2$  structure with 1/6 ML coverage is 0.7 eV [28], which compares favorably with the 0.9–1.0 eV gap measured in our work for Ca-induced structure. The lower saturation coverage for the Ba-induced reconstruction is also supported by a recent LEED and Auger electron spectroscopy study that reported 0.15 ML coverage for the “ $3 \times 1$ ” phase [35].

We have two indirect methods to measure the Ca coverage corresponding to the Ca- $3 \times 1$  structure, one based on the CaF<sub>2</sub> deposited, the other on the Ca 3p core-level intensity. 1/3 ML of CaF<sub>2</sub> is required for achieving a fully-saturated Ca- $3 \times 1$  after desorbing the F. The Ca 3p core-level intensity suggests 1/6 ML of Ca remaining on the surface, in qualitative agreement with the finding of 0.1 ML in Ref. [3]. That would imply desorption of 1/6 ML Ca together with the F.

While confirmation of the Ca coverage for the Ca- $3 \times 1$  by a more direct technique such as MEIS is desirable, the 1/6 ML coverage and the  $3 \times 2$  structure like in the Ba case is clearly an attractive possibility. One common property of both the Ba- and Ca-induced structures is their exceptional

stability at high temperature (up to 1050 °C [35] and  $\approx 925$  °C ([Section 2]) respectively). If the temperature stability of the alkaline earth induced HCC structure can be theoretically estimated as a function of metal coverage, it may prove to be a valuable test, since the observed stability surpasses that of the alkali-induced  $3 \times 1$  and is comparable to that of the Si- $7 \times 7$ .

A possibility of electron correlation or other many body effects has been previously suggested [8,33] to explain the unexpected non-metallic behavior of the alkaline earth  $3 \times 1$  systems. In fact the reduced metal coverage can be regarded as such an effect, whereby the energy of the semi-conducting state is low enough for the HCC structure, that the system undergoes a symmetry breaking from  $3 \times 1$  into  $3 \times 2$  and an associated change of metal coverage, rather than adjust the backbone structure. This is reminiscent of Au-induced anisotropic reconstructions, where an energetically preferred combination of the backbone and electronic structure of Si chains, drives structural and coverage changes between  $5 \times 1$  and  $5 \times 2$  reconstructions [1,36].

In conclusion, we have produced samples with single-domain Si(111) $3 \times 1$ -Ca reconstruction on vicinal surfaces. The topography and electronic structure of these samples were studied using STM and ARPES. The STM observations, in particular the ‘edge row’ structures on  $3 \times 1$  region boundaries, are consistent with the HCC model. The dispersions of two Ca- $3 \times 1$  surface states, identified in the ARPES data, are similar to predictions of the HCC model and published data for other  $3 \times 1$  systems. A gap of  $\approx 0.9$ – $1.0$  eV below  $E_F$  is reproducibly observed for the Ca- $3 \times 1$  surface in several ARPES configurations. The presence of this gap suggests that the HCC model developed from alkali metal induced  $3 \times 1$  data should be modified, with the recent suggestion of a  $3 \times 2$  structure with  $1/6$  ML metal coverage [28] being a very likely mechanism.

### Acknowledgements

This work was supported by the NSF under award nos. DMR-9815416 and DMR-0079983.

The photoemission experiments were carried out at the Synchrotron Radiation Center (University of Wisconsin—Madison), which is supported by the NSF under award no. DMR-0084402. We are grateful to J.N. Crain and A. Kirakosian for assistance with some of the experimental setup, and to S.C. Erwin (Naval Research Laboratory) and J.A. Carlisle (Argonne National Laboratory) for helpful discussions.

### References

- [1] F.J. Himpsel, K.N. Altmann, R. Bennewitz, J.N. Crain, A. Kirakosian, J.-L. Lin, J.L. McChesney, *J. Phys. Condens. Matter* 13 (2001) 11097.
- [2] H. Daimon, S. Ino, *Surf. Sci.* 164 (1985) 320; D. Jeon, T. Hashizume, T. Sakurai, R.F. Willis, *Phys. Rev. Lett.* 69 (1992) 1419; D. Jeon, T. Hashizume, T. Sakurai, *Jpn. J. Appl. Phys.* 32 (1993) 1423; H. Kleine, H. Bludau, H. Over, D. Fick, *Surf. Sci.* 410 (1998) 15.
- [3] M.A. Olmstead, R.I.G. Uhrberg, R.D. Bringans, R.Z. Bachrach, *J. Vac. Sci. Technol. B* 4 (1986) 1123; M.A. Olmstead, R.I.G. Uhrberg, R.D. Bringans, R.Z. Bachrach, *Phys. Rev. B* 35 (1987) 7526.
- [4] J. Quinn, F. Jona, *Surf. Sci.* 249 (1991) L307; C. Wigren, J.N. Andersen, R. Nyholm, U.O. Karlsson, *Surf. Sci.* 289 (1993) 290; H.H. Weitering, *Surf. Sci.* 355 (1996) L271.
- [5] K. Sakamoto, T. Okuda, H. Nishimoto, H. Daimon, S. Suga, T. Kinoshita, A. Kakizaki, *Phys. Rev. B* 50 (1994) 1725.
- [6] H.H. Weitering, X. Shi, S.C. Erwin, *Phys. Rev. B* 54 (1996) 10585.
- [7] A.A. Saranin, V.G. Lifshits, K.V. Ignatovich, H. Bethge, R. Kayser, H. Goldbach, A. Klust, J. Wollschlager, M. Henzler, *Surf. Sci.* 448 (2000) 87.
- [8] A.A. Baski, S.C. Erwin, M.S. Turner, K.M. Jones, J.W. Dickinson, J.A. Carlisle, *Surf. Sci.* 476 (2001) 22.
- [9] J. Viernow, J.-L. Lin, D.Y. Petrovykh, F.M. Leibsle, F.K. Men, F.J. Himpsel, *Appl. Phys. Lett.* 72 (1998) 948; J.-L. Lin, D.Y. Petrovykh, J. Viernow, F.K. Men, D.J. Seo, F.J. Himpsel, *J. Appl. Phys.* 84 (1998) 255; see also photoemission results for clean Si(111) $7 \times 7$  prepared by this method in R. Losio, K.N. Altmann, F.J. Himpsel, *Phys. Rev. B* 61 (2000) 10845.
- [10] D.Y. Petrovykh, J. Viernow, J.-L. Lin, F.M. Leibsle, F.K. Men, A. Kirakosian, F.J. Himpsel, *J. Vac. Sci. Technol. A* 17 (1999) 1415; J. Viernow, D.Y. Petrovykh, F.K. Men, A. Kirakosian, J.-L. Lin, F.J. Himpsel, *Appl. Phys. Lett.* 74 (1999) 2125.
- [11] A.B. Krasilnikov, A.V. Latyshev, A.L. Aseev, *Surf. Sci.* 290 (1992) 232.

- [12] G.C.L. Wong, C.A. Lucas, D. Loretto, A.P. Payne, P.H. Fuoss, *Phys. Rev. Lett.* 73 (1994) 991.
- [13] D. Rieger, F.J. Himpsel, U.O. Karlsson, F.R. McFeely, J.F. Morar, J.A. Yarmoff, *Phys. Rev. B* 34 (1986) 7295; A.B. McLean, F.J. Himpsel, *Phys. Rev. B* 39 (1989) 1457.
- [14] K.J. Wan, X.F. Lin, J. Nogami, *Phys. Rev. B* 46 (1992) 13635.
- [15] R.J. Wilson, S. Chiang, *Phys. Rev. Lett.* 58 (1987) 369.
- [16] C. Wigren, J.N. Andersen, R. Nyholm, U.O. Karlsson, J. Nogami, A.A. Baski, C.F. Quate, *Phys. Rev. B* 47 (1993) 9663.
- [17] C. Wigren, J.N. Andersen, R. Nyholm, M. Gothelid, M. Hammar, C. Tornevik, U.O. Karlsson, *Phys. Rev. B* 48 (1993) 11014.
- [18] C. Wigren, J.N. Andersen, R. Nyholm, U.O. Karlsson, *Surf. Sci.* 293 (1993) 254.
- [19] D. Jeon, T. Hashizume, T. Sakurai, *J. Vac. Sci. Technol. B* 12 (1994) 2044; S. Olthoff, A.W. McKinnon, M.E. Welland, *Surf. Sci.* 326 (1995) 113; S. Olthoff, M.E. Welland, *J. Vac. Sci. Technol. B* 14 (1996) 1019.
- [20] C. Collazo-Davila, D. Grozea, L.D. Marks, *Phys. Rev. Lett.* 80 (1998) 1678.
- [21] L. Lottermozer et al., *Phys. Rev. Lett.* 80 (1998) 3980.
- [22] W.C. Fan, A. Ignatiev, *Phys. Rev. B* 41 (1990) 3592.
- [23] T. Okuda, H. Shigeoka, H. Daimon, S. Suga, T. Kinoshita, A. Kakizaki, *Surf. Sci.* 321 (1994) 105.
- [24] H.H. Weitering, N.J. DiNardo, R. Perez-Sandoz, J. Chen, E.J. Mele, *Phys. Rev. B* 49 (1994) 16837.
- [25] A.A. Saranin, A.V. Zotov, V.G. Lifshits, J.-T. Ryu, O. Kubo, H. Tani, T. Harada, M. Katayama, K. Oura, *Phys. Rev. B* 58 (1998) 3545.
- [26] S. Hasegawa, M. Maruyama, Y. Hirata, D. Abe, H. Nakashima, *Surf. Sci.* 405 (1998) L503.
- [27] S.C. Erwin, H.H. Weitering, *Phys. Rev. Lett.* 81 (1998) 2296.
- [28] G. Lee, S. Hong, H. Kim, D. Shin, J.-Y. Koo, H.-I. Lee, D.W. Moon, *Phys. Rev. Lett.* 87 (2001) 056104.
- [29] M.A. Olmstead, in: A.W.K. Liu, M. Santos (Eds.), *Heteroepitaxial Systems*, World Scientific, Singapore, 1998 (Chapter 5).
- [30] R.I.G. Uhrberg, G.V. Hansson, *Crit. Rev. Solid State Mat. Sci.* 17 (1991) 133.
- [31] A.A. Saranin, A.V. Zotov, V.G. Lifshits, M. Katayama, K. Oura, *Surf. Sci.* 426 (1999) 298.
- [32] K.S. An, R.J. Park, J.S. Kim, C.Y. Park, C.Y. Kim, J.W. Chung, T. Abukawa, S. Kono, T. Kinoshita, A. Kakizaki, T. Ishii, *Surf. Sci.* 337 (1995) L789.
- [33] E. Rotenberg, private communication; J. Schafer, E. Rotenberg, S.D. Kevan, in press.
- [34] O. Kubo, A.A. Saranin, A.V. Zotov, J.-T. Ryu, H. Tani, T. Harada, M. Katayama, V.G. Lifshits, K. Oura, *Surf. Sci.* 415 (1998) L971.
- [35] T. Urano, K. Watanabe, S. Hongo, *Appl. Surf. Sci.* 169 (2001) 88.
- [36] R. Losio, K.N. Altmann, F.J. Himpsel, *Phys. Rev. Lett.* 85 (2000) 808; R. Losio, K.N. Altmann, A. Kirakosian, J.-L. Lin, D.Y. Petrovykh, F.J. Himpsel, *Phys. Rev. Lett.* 86 (2001) 4632; K.N. Altmann, J.N. Crain, A. Kirakosian, J.-L. Lin, D.Y. Petrovykh, F.J. Himpsel, R. Losio, *Phys. Rev. B* 64 (2001) 035406.